



A New In Situ Test for the Assessment of the Rock-Burst Alarm Threshold During Tunnelling

A. Voza¹ · L. Valguarnera¹ · R. Marrazzo¹ · G. Ascari² · D. Boldini³ 

Received: 10 April 2022 / Accepted: 7 November 2022
© The Author(s) 2022

Abstract

Rock-burst is one of the most serious risks associated with hard rock tunnelling and mining at high depths. Monitoring of acoustic emissions emitted by the rock-mass during excavation and their interpretation now permits the early assessment of failure events and makes the safe management of the construction works possible. A reliable set-up of the alarm threshold is thus fundamental for the correct implementation of the procedures planned to minimise rock-burst related risk. This paper focuses on a novel in situ test specifically developed to provide an experimental basis for a more accurate assessment of the alarm threshold during tunnelling, representative of the local geomechanical conditions. The test, thanks to the compression induced by two flat jacks at the tunnel side wall, produces an artificial failure process during which acoustic emissions are measured and correlated to the mechanical response of the rock-mass, without the typical limitations of scale that characterised the laboratory experiments. The new methodology, named the Mules method, was successfully tested during the excavation of some stretches of the Brenner Base Tunnel in the Brixner granite, affected by mild spalling episodes. The case-history is fully described in the paper to illustrate the practical application of the proposed approach.

Highlights

- A new in situ test is proposed for the assessment of the rock-burst alarm threshold.
- The rock-mass is brought to failure at the tunnel side wall by two flat jacks and acoustic emissions are monitored.
- Two tests were carried out during the construction of the Brenner Base tunnel in a granite formation under high cover affected by mild spalling phenomena.
- The power spectrum density of the signals recorded during the tests displayed its maximum values before the rock-mass failure.
- Test results interpreted in terms of power spectrum density summation were adopted to set up the rock-burst alarm threshold during tunnel excavation.

Keywords Rock-burst · Spalling · Acoustic emission · Alarm threshold · In situ test · Brenner Base Tunnel · The Mules method

1 Introduction

Tunnelling or mining in hard rocks at high depths is potentially affected by rock-burst phenomena of different intensity (i.e. spalling, strain-burst) (Ortlepp and Stacey 1994; Diederichs 2007; ITA 2017; Cai and Kaiser 2018) that can seriously put worker safety at risk and can certainly produce construction delays and increased costs (e.g. Brauner 1994; Cai 2013; Zhang et al. 2013; Naji et al. 2019). In China alone, a significant increase in the number of coal mines reporting rock-burst hazards has been observed,

✉ D. Boldini
daniela.boldini@uniroma1.it

¹ Galleria di Base del Brennero–Brenner Basistunnel BBT-SE, Bolzano, Italy

² Akron S.r.l, Bovisio Masciago, Italy

³ Department of Chemical Engineering Materials Environment, Sapienza University of Rome, Via Eudossiana 18, 00184 Rome, Italy

rising from 32 in 1985 to more than 253 by the end of 2019 (Cai et al. 2020). This hazard is continuously monitored during excavation by measurement and interpretation of the micro-seismic activity typically associated with the release of the elastic energy stored in the rock-mass (Kaiser et al. 1996; Mendecki 1997). Since the warning time is relatively short, automatic alarm thresholds are typically set up to activate the procedures implemented for the management of the construction activities in view of a potential rock-burst episode. However, it should be pointed out that it is not generally feasible to exactly predict the occurrence of the phenomenon, as the monitoring interpretation mostly provides information about its location and intensity (Feng and Feng 2018).

This paper describes a new in situ test specifically developed to experimentally support the selection of the rock-burst alarm threshold during tunnelling (the term rock-burst is used here and in the following to generically refer to fragile failure phenomena in the rock-mass, both in the form of proper rock-burst episodes or milder spalling events). The test is aimed at reproducing the in situ rock-mass failure while measuring the related acoustic emissions with accelerometric sensors. It has already been implemented twice during the construction of a stretch of the Brenner Base Tunnel (hereafter known as BBT) already identified as at risk during the design stage (because of the high depth, over 1000 m and the presence of a hard rock, Brixner granite) and actually affected by few mild spalling events. In the experiments, failure was induced by the compression of two flat jacks at the tunnel side-wall, but other systems are in principle possible. Test results, interpreted in terms of cumulated power spectrum density over a specific time window, were useful to calibrate the alarm threshold of the monitoring system so as to define an integrated strategy for risk management in combination with a careful evaluation of monitoring data and of tunnel performance.

After a brief literature review of the main approaches adopted for rock-burst monitoring and alarm threshold assessment, the new in situ test is introduced from a theoretical point of view. The practical application of the experimental methodology is then described with reference to the case history of the BBT project, with insight into the monitoring system and collected measurements over 3 years and almost 5 km of excavation. The characteristics of the rock-mass at the two test locations, detected by means of in situ surveys and laboratory tests conducted on the rock material, are discussed in detail. The final part of the paper focuses on the so-called “Mules method”, a comprehensive approach for the safe management of the tunnel construction in rock-burst risk-prone areas.

2 Literature Review

In this paragraph the focus is on the monitoring techniques implemented during tunnelling and mining activities for the monitoring and early warning of rock-burst occurrence.

Several techniques are adopted nowadays, often in combination, for continuous monitoring of the rock-mass response during excavation (e.g. Mendecki 1997; Ge 2005; Dou et al. 2018; Cai et al. 2020). They include microseismic (MS) monitoring, electromagnetic radiation (EMR) and acoustic emission (AE), this latter being the technique discussed in this paper. For many of them there already exists a sufficiently long experience of use in the coal mining industry, due to the high risk associated to this activity which is often carried out at depths greater than 2000 m. The common background relies on the fact that rock-burst events are anticipated by various types of dynamic precursor information, the collection and interpretation of which is useful at a predictive stage.

MS measurement, since the first studies in South Africa (Cook 1963) and the US (Obert 1975), is the most diffuse monitoring system, providing information on times, locations, intensities and mechanisms of the rock-fracturing processes. The spatial distribution of MS events, for example, is clearly characterised by a nucleation process which points out the location of the potential rock-burst event (e.g. Li et al. 2012). Some authors (e.g. Feng et al. 2016) have also revealed that rock-burst episodes display self-similarity, i.e. a spatial and temporal fractal behaviour.

EMR is a no-contact technique aimed at detecting electron emission and the associated electromagnetic radiation during rock cracking and fracturing (Frid 2001; Frid and Vozoff 2005). Traditional EMR technology has mainly focussed on the study of medium–high frequency ranges (300 kHz ~ 30 MHz), with problems related to the disturbance produced by the underground electromechanical devices and to the rapid attenuation of the signals. Qiu et al. (2020) demonstrated that low-frequency EMR signals (1 kHz) are more sensitive to the response of local fractures and can be regarded as the precursor of rock-burst disasters in coal mines.

AE technique, after the pioneer work of Kaiser (1950), is nowadays extensively employed in laboratory experiments on rocks to continuously detect, in time and space, the generation, propagation and coalescence of micro-cracks during compression and tensile tests (e.g. Kao et al. 2011; Liu et al. 2020a, b) as well as to identify the different failure modes (Du et al. 2020). Application of AE studies to larger scale problems, including rock-burst forecasting, was later introduced, among others, by Hardy (1981), Kuksenko et al. (1982, quoted in Frid 2001) and Mansurov (1994). In fact, based on the observations by Lockner (1993) about the strong

correlation existing between the Gutenberg-Richter law for seismic events (produced by earthquakes as well as by rock-bursts typically characterised by large magnitude and small frequency) and the frequency–magnitude relationship for AE events (for which high frequency and small magnitude are expected), it was suggested that micro-shocks are precursors of macro-failure (Frid 2001). A more recent application of this technique can be found in Cheng et al. (2013).

Many authors have used MS monitoring data to warn of rock-burst occurrence, typically adopting multiple seismic parameters (e.g. Alcott et al. 1998; Liu et al. 2013), integrated if possible with other information related to the state of stress or rock-mass characteristics. On the basis of the ample and long-term dataset collected during the construction of a number of deep tunnels for the Jinping II hydropower station, real-time warning strategies, including the indication of the event intensity (i.e. extremely intense, intense, moderate and slight), were proposed by Feng et al. (2015) and Feng et al. (2019), this latter adopting an optimised probabilistic neural network. For the same case-history, Feng et al. (2020) implemented a cluster analysis to formulate a warning method also in presence of a limited number of rock-burst events, as occurring in the initial period of MS monitoring. Specifically, for drill-and-blast tunnelling Feng and Feng (2018) suggested considering the following MS parameters: (1) cumulative number of microseismic events, (2) cumulative microseismic energy, (3) cumulative microseismic apparent volume, (4) microseismic event rate, (5) microseismic energy rate and (6) microseismic apparent volume rate, the rate quantities being expressed for day or hour. He et al. (2022), also by comparing MS observations in coal-rock parting-coal structure in a coal mine and representative laboratory tests, identified a number of rockburst precursors and their evolution during failure mechanisms, i.e. a sharp decline in the energy index, a sharp rise in the cumulative apparent volume and an increase in MS at a low frequency and high amplitude.

The selection of the proper alarm thresholds probably represents the most difficult and uncertain step in proficient management of the rock-burst risk. Alcott et al. (1998) described three case studies located at different blocks of the sulphide ore Brunswick mine. Thresholds for the selected criteria, namely the energy, apparent stress and seismic moment, were first empirically established at one location and later calibrated at the other two, demonstrating the robustness of the proposed approach. More recently, Yu et al. (2021), analysing 40 rock-burst events of different intensities at the Jinping-II hydropower station, identified quantitative risk thresholds using the local energy release rate and energy

fractal dimension of MS events. For the same case-history, Liang et al. (2020) tested five machine learning algorithms for assessing the short-term rock-burst risk, which were found to efficiently predict none, moderate and intense events.

3 The New In Situ Test

The new in situ test was developed with the idea of bringing the rock-mass to failure in a controlled manner, to accurately detect the evolution in intensity and frequency of the emitted acoustic emissions and relate them to the ongoing failure process. Essentially, the principle is similar to that adopted in the laboratory for rock materials, with the main difference of referring to the same material, the rock-mass, potentially affected by fragile failure phenomena, so as to significantly limit the scale effect. The tested volume of rock-mass, in fact, may include fractures and/or other inhomogeneities thus reflecting the nature of the material encountered during the excavation. Obviously, as for any in situ experimental programme characterised by a relatively small volume in comparison to the tunnel size, reliable results could require the execution of several tests depending on the level of anisotropy and joint spacing properties of the rock-mass.

The testing procedure should include the definition of the instrumentations for the load application and of the acquisition systems for the mechanical as well as acoustic parameters of interest. The experimental activity was designed in such a way as to: (1) not be excessively expensive, (2) not interfere with the tunnelling operation and (3) use standard equipment typically available at the construction site for other in situ tests or monitoring systems. With reference to these aspects, the option explored in this research was that of using a couple of flat jacks to compress, ideally to failure, the rock-mass at the tunnel side-wall while simultaneously measuring the related acoustic emissions by accelerometric and velocimetric sensors placed at the rock surface (Fig. 1). These latter should provide quantitative information compatible to that used for the interpretation of the rock-burst monitoring data continuously acquired during tunnelling, as discussed in the paper. In the following, the adopted quantity, i.e. the power spectrum density summation, will be defined in detail. Non-essential ingredients of the test, which are nonetheless useful to improve its understanding, are the measurement of displacements, which can provide a better insight into the mechanical response of the rock-mass and the frequency and automatization of the readings, especially useful for plotting the force–displacement curve and for a better correlation in time with the acoustic emission data.

Fig. 1 Sketch of the newly proposed in situ test

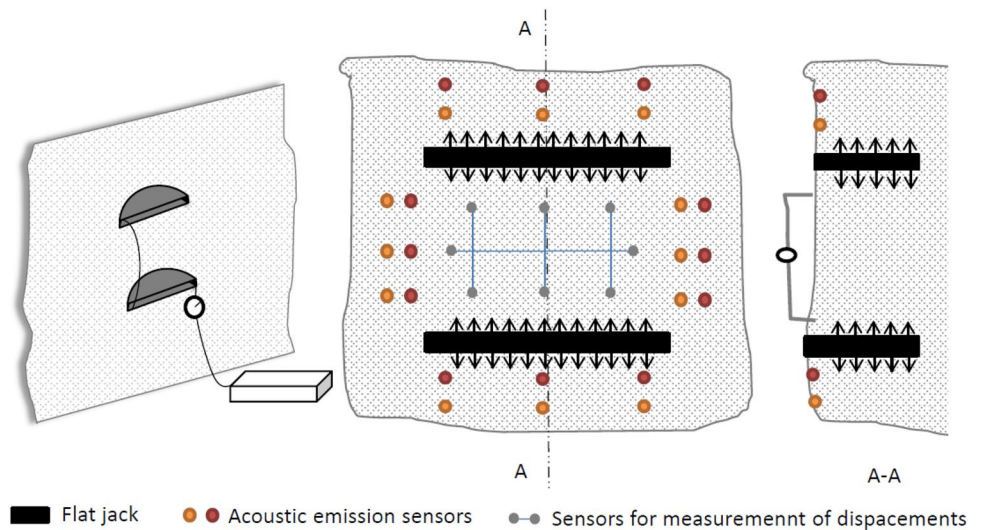
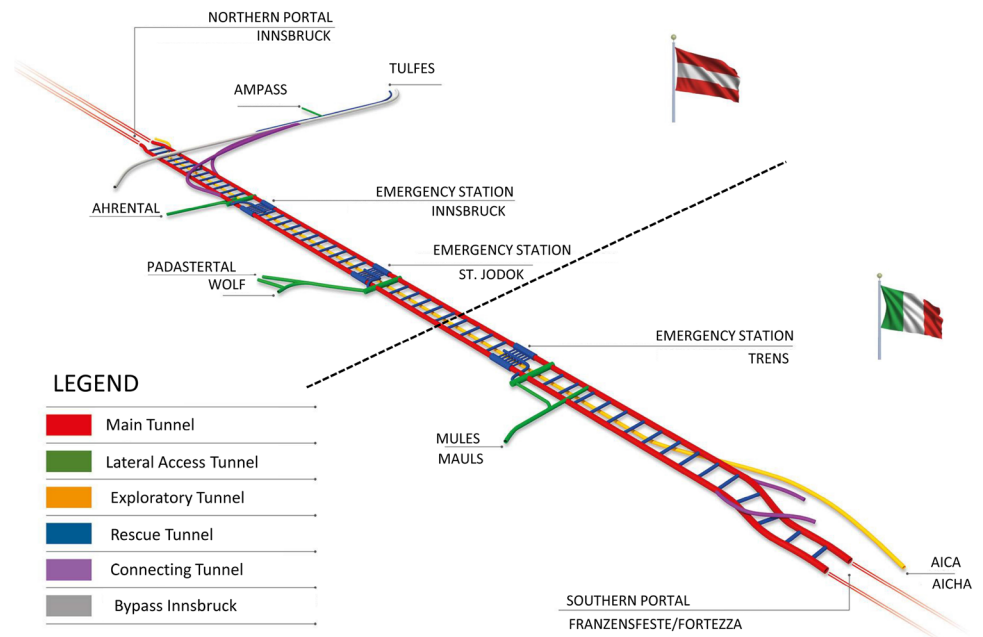


Fig. 2 Sketch of the Brenner Base Tunnel underground system



4 The Experience of the Brenner Base Tunnel

The Brenner Base Tunnel is a complex railway underground system through the Alps belonging to the so-called Scandinavian–Mediterranean Corridor of the Trans-European Transport Network. When completed in 2028, according to the current schedule, it will connect the cities of Innsbruck (Austria) and Fortezza (Italy) for a total length of 55 km (Fig. 2), contributing significantly to shift freight transport from road to rail.

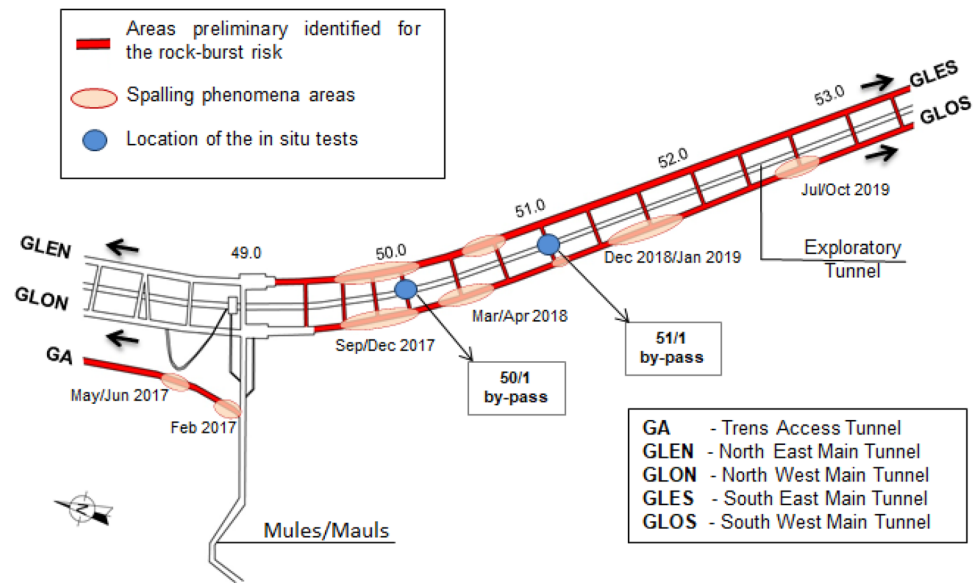
The experimental sites were located in the southern portion of the construction works excavated in the Brixner

granite formation at high depths (e.g. Boldini et al. 2018; Foderà et al. 2020), for which rock-burst risk was identified at the design stage.

4.1 The Brixner Granite and the Rock-Burst Related Risk at the Design Stage

The BBT tunnels cross the main tectonic units of the Alpine chain; however, the area under investigation lies entirely in the Brixner granite unit (Fig. 3). It includes the main single-direction railway tunnels directed southward, referred to as GLES and GLOS (respectively the eastern and western tunnels), having a diameter of about 9.3 m and a portion of the

Fig. 3 Layout of the southern portion of the BBT system in the Brixner granite. Red zones highlight the areas identified for the rock-burst risk before the construction



access tunnel known as GA, whose diameter is 9.2 m, all excavated at depths higher than 1000 m (Table 1).

The rock material was characterised by an extensive laboratory campaign that identified the following mean values for the principal physical–mechanical properties: quartz content 72%, unit weight of volume 26.6 kN/m³, porosity 0.78%, P-wave velocity 4299 m/s, Point Load strength index 4.8 MPa, uniaxial compressive strength 140 MPa and related Young’s modulus 36 GPa. According to the Deere–Miller classification the material is thus a high-strength rock (class B) with a medium modulus ratio (MR = 257).

The main characteristics of the rock-mass encountered during the excavation of the GLES and GLOS tunnels are summarised in Table 1 as a function of the chainage, inferable from Fig. 3. The Hoek–Brown strength properties of the rock-mass were calculated from those of the rock material based on the GSI value, adopting a disturbance factor $D=0.7$, while the Young’s modulus was estimated following Hoek and Diederichs (2006). It is evident that, except for two short stretches, the uniaxial compressive strength of the rock material σ_{ci} is on average well above 100 MPa and

the quality of the rock-mass in terms of RMR quality ranges from good to very good.

The criteria of Tao (1988) and of Hoek and Brown (1980) were adopted to assess the rock-burst risk at the design stage. The first one considers the ratio of the uniaxial compressive strength of the rock material to the maximum principal stress, σ_{ci}/σ_1 . In the second case the ratio σ_v/σ_{ci} is evaluated, in which the term at the numerator is the vertical stress at the tunnel depth. For all the red areas of Fig. 3 a mild rock-burst risk was estimated considering the Tao approach, while severe spalling was predicted according to the Hoek and Brown criterion. As such, it was decided to perform the excavation under the strict control of an acoustic emission monitoring system, as described in the following paragraph.

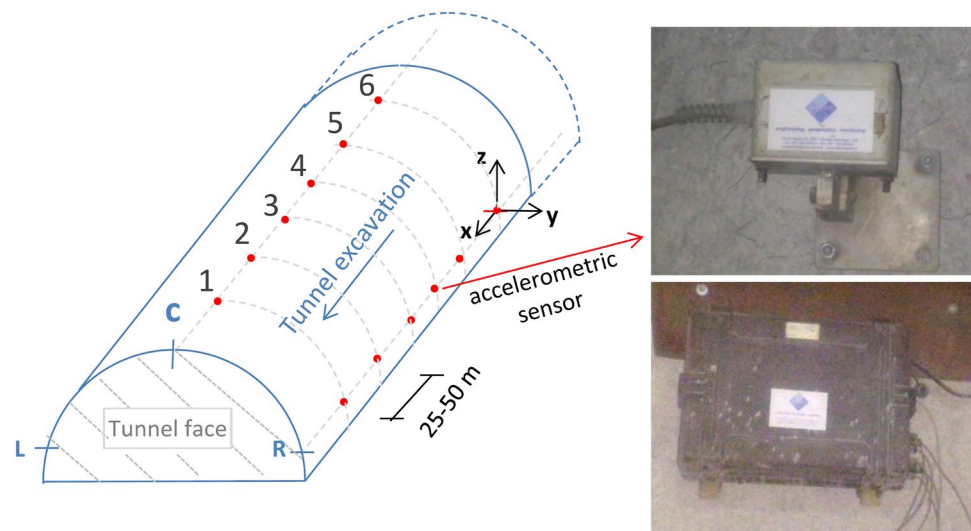
4.2 Monitoring of the Acoustic Emissions During the Excavation

Acoustic emissions were measured during tunnel excavation by highly sensitive piezoelectric triaxial accelerometric ICP (integrated circuit piezoelectric) sensors. These were installed in groups of three along six monitoring sections

Table 1 Principal rock-mass characteristics along the GLES and GLOS tunnels

GLES		GLOS		Depth min/max (m)	RMR	GSI	σ_{ci} (MPa)	m_b [-]	E (GPa)
Chainage (m)		Chainage (m)							
49+081	50+322	49+093	50+348	1085–1295	73 ± 11	52–50	115 ± 19	1.54–1.72	28.6
50+322	50+394	50+348	50+420	1275	52 ± 11	42	89 ± 18	0.91	11.9
50+394	51+564	50+420	51+590	1150–1350	72 ± 13	21–52	131 ± 27	0.31–1.72	24.7
51+564	51+706	51+590	51+732	1150	59 ± 8	43	90 ± 18	0.96	13.1
51+706	52+374	51+732	51+400	975–1150	66 ± 11	50–52	122 ± 28	1.54–1.72	23.0
52+374	54+026	52+400	54+052	80–1000	60 ± 10	50–64	122 ± 28	1.54–3.32	23.7

Fig. 4 Details of the acoustic emission monitoring system (modified from Voza et al. 2020a). The sensor positions along the section are indicated with L, C and R; the monitoring sections are numbered from 1 to 6 for increasing distances from the tunnel face



located at progressive distances of 25–50 m from the tunnel face (Fig. 4).

Signals were recorded at a sampling rate of 2000 Hz and processed in the frequency domain, considering fixed intervals of 10 min. Based on previous experiences (e.g. Padovese et al. 2017), frequencies in the range of 500–1000 Hz were considered as associated with pre-failure acoustic emissions related to rock-burst and spalling. In fact, the frequency content of acoustic emissions generated by rock-mass failure is typically significantly lower than that observable for metallic materials (i.e. higher than 20 kHz). In addition, the higher frequency content of the signal is very rapidly absorbed within few metres from the emission source, thus making possible from a practical point of view the sole measurement of the lower frequency content associated with those emissions. On the other side, the lower cut-off of 500 Hz is useful to avoid the interference with other measurable vibration phenomena, including those due to blasting, characterised by lower frequency ranges.

Monitoring data were interpreted in terms of power spectrum density (PSD), correlated to the energy emitted by the rock-mass during the failure phenomena occurring as a consequence of the tunnelling-induced stress redistribution. For each 10-min time interval T , the power spectrum density was calculated for each frequency f_n of the considered frequency range 500–1000 Hz from the related Fourier spectrum as follows:

$$PSD(f_n) = \frac{1}{2} \frac{(a_n^2 + b_n^2)}{\Delta f} \quad (1)$$

where a_n and b_n are the Fourier coefficients and Δf is the frequency resolution, equal to 1 over T . This quantity can be considered an indicator of the signal power content in the frequency domain.

The real-time assessment of the rock-burst related risk was based on the so-called power spectrum density summation $PSDS$, obtained by taking the maximum value of PSD of each time interval and adding it to with the corresponding quantities extrapolated along the previous time intervals:

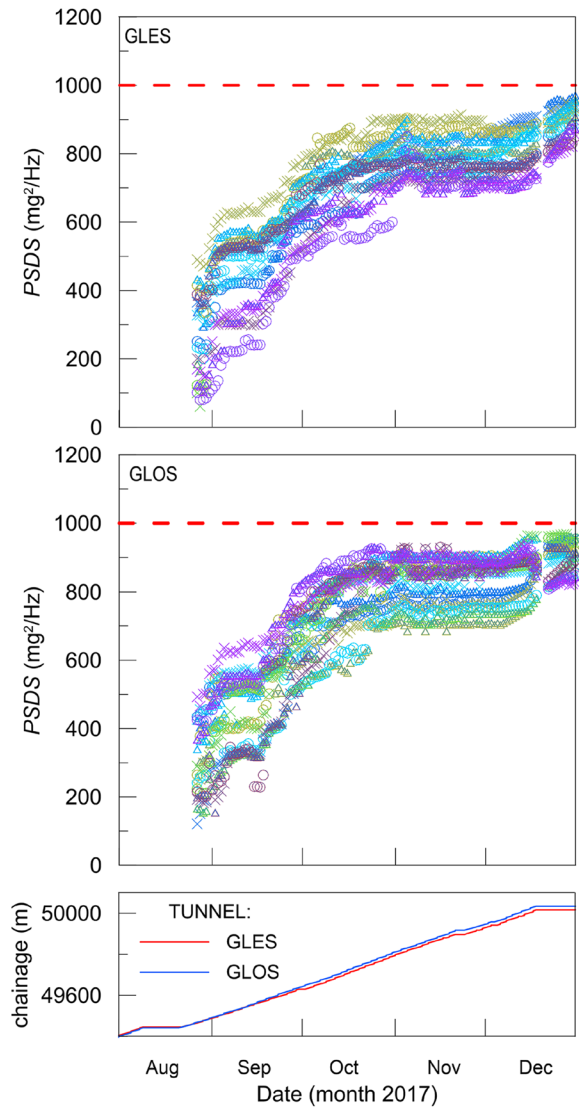
$$PSDS = \sum_{i=1}^N PSD_{max,i} \quad (2)$$

where PSD_{max} is the maximum value of PSD in the 10-min interval and N is the total number of considered time intervals. The selection of this risk indicator, already adopted during the excavation of the Maddalena exploratory tunnel in the Turin–Lyon connection project (Padovese et al. 2017), is due to the need to assess the evolution of PSD over time. The $PSDS$ quantity will be heretofore expressed in $(\text{mg})^2/\text{Hz}$.

In the BBT, different time windows were selected over the years. A time window of 24 h was first selected for the year 2017 (corresponding to a value of N equal to 144, obtained by multiplying 24 h by 6 intervals of 10 min each). Then, after the occurrence of the first spalling phenomena not captured by the $PSDS$ evolution in time (see the episodes from September to December 2017 in Fig. 3), it was decreased to 12 h in 2018 (N equal to 72) and to 6 h in 2019 (N equal to 36). $PSDS$ values of 2018 and 2019 are therefore intrinsically lower than those of the year 2017 (i.e. exactly one half and one quarter for the same accelerometric input) because of the different time interval adopted.

Figures 5, 6 and 7 summarise all the $PSDS$ values calculated during the excavation of the stretches of the BBT tunnels classified at risk occurred from 2017 to 2019 (Voza et al. 2020b). A log of the position of the two tunnel faces in time is also plotted. In general, slightly larger values of $PSDS$ were recorded in the GLES tunnel, the first one to be excavated and to likely produce a more significant perturbation

Fig. 5 Tunnel advancement log and related acoustic emission data in terms of *PSDS* collected during the year 2017. The legend refers to the sensor position illustrated in Fig. 4



of the in situ state of stress. Inspection of figures reveals also that the *PSDS*, after an initial stable increase till the beginning of 2018, was characterised by large fluctuations since May 2018. These were followed by an almost constant trend in the following months of 2018, with a clear reduction in the peaks during the summer break. More significant acoustic emission activity can be observed at the beginning of 2019 due to the already mentioned spalling phenomena affecting the tunnel construction (see Fig. 3 for the location of the events). Finally, the last four months of 2019 showed high values of the *PSDS* values associated with sensor 1C only, imputable to its malfunctioning.

4.3 Description of the Experimental Sites and Equipment

The two in situ tests were conducted in two by-passes between the GLES and GLOS tunnels (see Fig. 8a) at chainages 50 + 000 (50/1 by-pass) and 51 + 000 (51/1 by-pass). The tunnel connections are characterised respectively by an area of 25.68 m² and 43.79 m², corresponding to an equivalent radius of 2.68 m and 3.73 m. In particular, the first one was carried out in the 50/1 by-pass in February 2018 (Valguarnera 2018; Voza et al. 2019), while the second test took place in the 51/1 by-pass 1 year later (Siboni 2019).

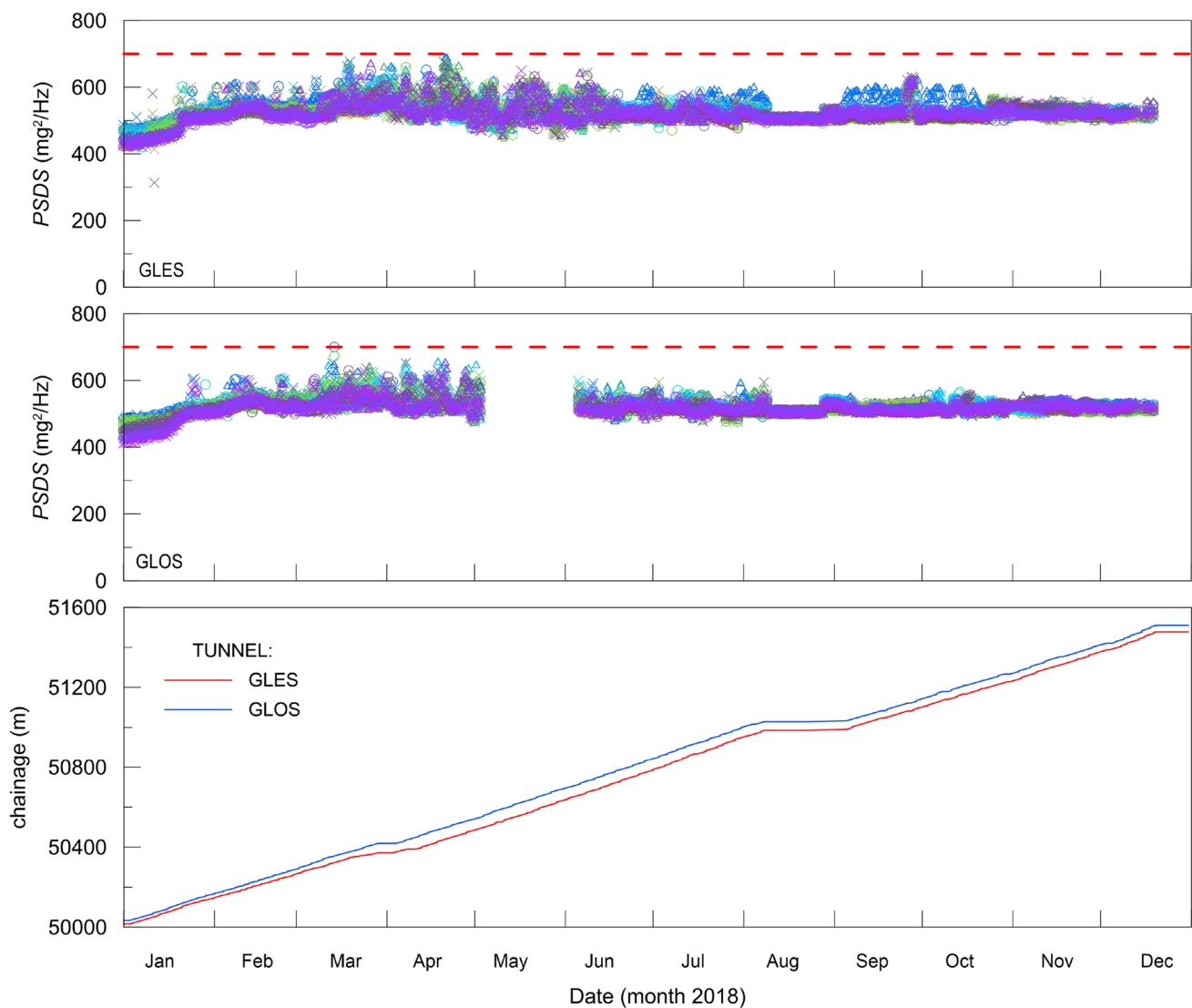


Fig. 6 Tunnel advancement log and related acoustic emission data in terms of *PSDS* collected during the year 2018 (for the symbols refer to the legend of Fig. 5)

4.3.1 Rock-Mass Characteristics

A detailed survey of the rock-mass characteristics was carried out at the by-pass surface before the in situ test execution. As summarised in Table 2, the rock-mass is in both cases of very good quality and affected by three joint sets, whose fractures are closed, persistent, unweathered and with no infilling. The *JRC* roughness parameter is between 4 and 6 for the joints at the 50/1 by-pass, while it can reach 8 for one joint set of the 51/1 by-pass. No water inflow was observed at the two sites.

4.3.2 Laboratory Tests on the Rock Material

To characterise the mechanical properties of rock material at the two in situ test sites, several cores were recovered from the by-pass side walls with a manual electrical drilling rig. Figure 9 shows the collected cores. More specifically, the four cores sampled at the 50/1 by-pass have a diameter of about 84 mm (Fig. 9a), while for the 51/1 by-pass, one core of about 84 mm and four cores of about 51 mm in diameter were available (Fig. 9b).

Cylindrical specimens were prepared for uniaxial compression and Brazilian tests. For the material collected in the

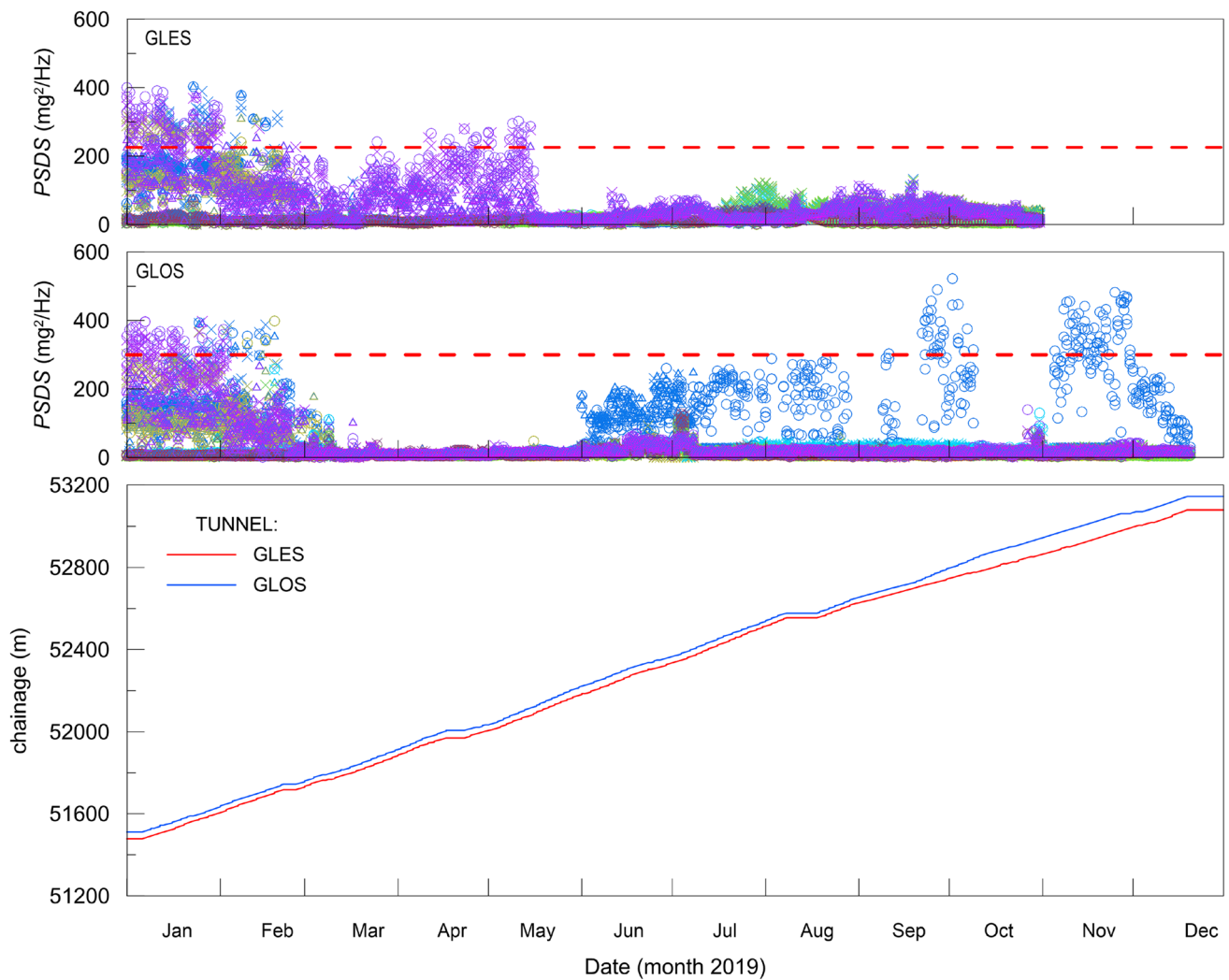


Fig. 7 Tunnel advancement log and related acoustic emission data in terms of *PSDS* collected during the year 2019 (for the symbols refer to the legend of Fig. 5)

50/1 by-pass, coring of the original samples was required due to the presence of some fractures and cavities near the lateral surfaces and to their limited length. In particular, the 51 mm in diameter cores were reduced to a diameter of about 38 mm for the uniaxial compression specimens, while two specimens of 54 mm in diameter were prepared for the Brazilian tests.

Solid matrix density, ρ_s , was determined with a pycnometer on ground rock fragments passing the No. 230 (63 μm) ASTM E11 sieve, obtaining a mean value of 2.698 and 2.720 Mg/m^3 , respectively for the two sites. Total porosity, n and effective porosity, n_w , were assessed using the weights of the saturated-surface-dry (after having saturated them for

24 h) and oven-dry specimens. For those specimens lacking a direct determination of n , the value was calculated from the mean value of solid matrix density and from dry density, ρ_{dry} , of specimens oven-dried at 70 °C. Finally, ultrasonic velocities of longitudinal, V_p and shear, V_s , waves were evaluated on dry and saturated specimens (in this latter case only the P wave transit time was obviously recorded) by measuring the transit time of a square wave.

All data are summarised in Table 3. The significant difference in porosity of the two sets of specimens is evident, with values more than three times larger for the material collected in the 50/1 by-pass. In particular, specimens 50/1-1C and 50/1-1D show values of n over 3%, due to the presence

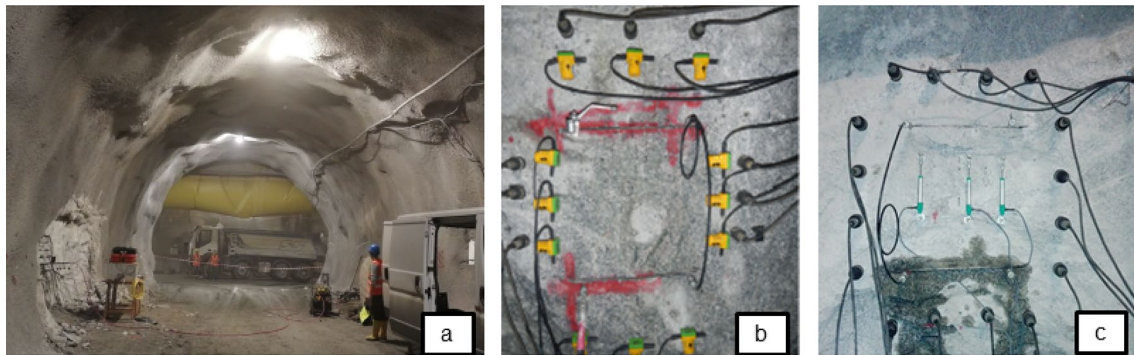
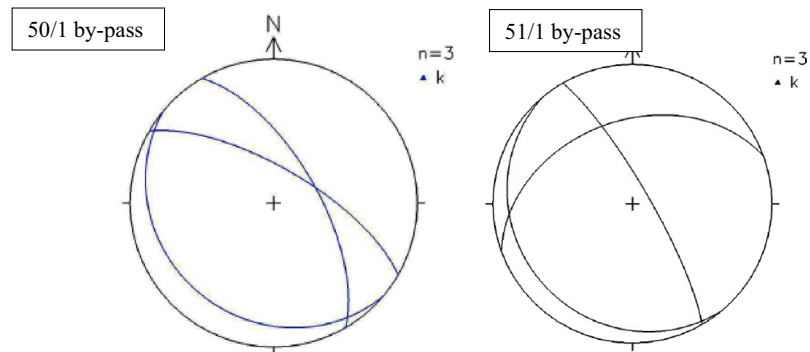
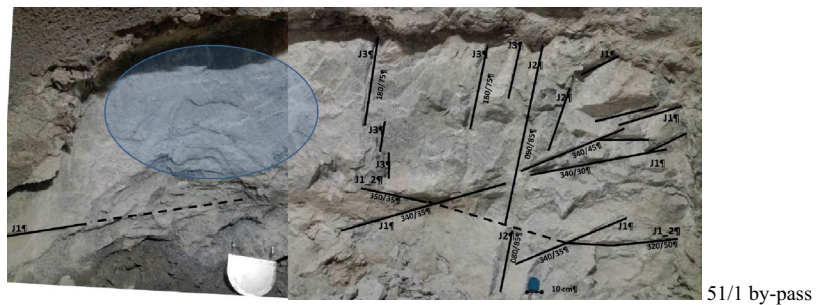


Fig. 8 In situ test performed in the 50/1 by-pass: **a** general view, **b** test set up 50/1 by-pass and **c** test set up 51/1 by-pass (the two flat jacks MP1 and MP2 and the acoustic emission sensors are visible)

of fractures. The better quality of the Brixner granite of the second site (i.e. 51/1 by-pass) is also clearly highlighted by the values of ultrasonic velocities, plotted in Fig. 10 as a function of porosity. The average values of V_p and V_s are

respectively equal to 4.8 and 2.9 for 51/1 by-pass specimens, while they reduce to 3.9 and 2.6 for the 50/1 by-pass ones. Saturation induces a not negligible increase in the P-wave velocities for both sets, the higher the larger the porosity

Table 2 Characteristics of the rock-mass at the by-pass surfaces before the in situ tests



	50/1 by-pass			51/1 by-pass		
Depth H (m)	1200			1300		
Joint	1	2	3	1	2	3
Dip direction/dip ($^{\circ}$)	060/65	220/20	030/70	230/15	060/80	340/40
Spacing (mm)	600-2000	2000-6000	>6000	600-2000	600-2000	600-2000
Persistency (m)	3-10	3-10	1-3	3-10	3-10	3-10
Roughness (JRC)	4-6	4-6	4-6	6-8	4-8	4-8
Infilling	None	None	None	None	None	None
Weathering	Unweathered	Unweathered	Unweathered	Unweathered	Unweathered	Unweathered
Separation (mm)	<0.1	<0.1	<0.1	<0.1	<0.1	<0.1
RMR_{89}	86			80		
GSI	80			75		

Fig. 9 Cores recovered from the areas of the in situ tests: **a** 50/1 and **b** 51/1 by-pass

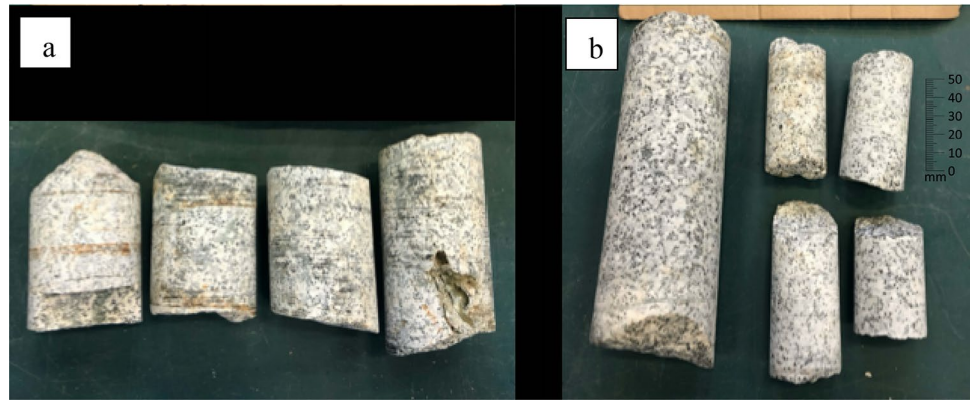


Table 3 Principal characteristics of the Brixner granite specimens ($\langle x \rangle$ =mean value, sd =standard deviation, N =number of data, $E_{t,50}$ and $E_{s,50}$ =tangent and secant Young’s modulus at 50% of the maximum applied load) (modified from Marrazzo 2020)

	ρ_{dry} (Mg/m ³)	ρ_{sat} (Mg/m ³)	n (%)	n_w (%)	Dry		Saturated	σ_t (MPa)	σ_c (MPa)	$E_{t,50}$ (GPa)	$E_{s,50}$ (GPa)
					V_p (km/s)	V_s (km/s)	V_p (km/s)				
50/1 by-pass											
$\langle x \rangle$	2.627	2.626	2.60	2.45	3.9	2.6	5.4	10.2	150.3	55.4	44.9
sd	0.012	0.030	0.47	0.95	0.3	0.5	0.1	0.9	55.1	5.2	2.6
N	6	6	6	6	6	6	6	2	4	2	2
51/1 by-pass											
$\langle x \rangle$	2.680	2.667	1.47	0.54	4.8	2.9	5.8	10.2	199.7	75.0	59.2
sd	0.008	0.015	0.32	0.14	0.3	0.1	0.1	2.2	24.9	10.7	4.8
N	7	7	7	7	7	7	7	4	3	3	3

(and, as such, particularly significant for the two specimens of the 50/1 by-pass having a n value larger than 3%).

Brazil tests, carried out with a servo-electric press of 50 kN, provided a mean value of the tensile strength equal to about 10 MPa for both groups (see Table 3), likely because no 50/1 specimens with porosity larger than 3% were available. Figure 11 reveals that, despite the reduced number of determinations, a small increase in porosity produces a significant drop in the tensile strength values.

The results of the uniaxial compression tests, carried out with a servo hydraulic press by increasing the axial stress of 0.5 MPa/s, are summarised in Table 3, which also includes the Young’s modulus and Poisson’s ratio estimated for those specimens instrumented with strain gauges (this was not possible for specimens 1C and 1D because of the presence of numerous fractures). More specifically, the stiffness properties of Table 3 are provided as tangent and secant values at 50% of the maximum applied load. Again, it is evident that the material sampled in the 51/1 by-pass is characterised by significantly better mechanical behaviour, both in terms of strength and stiffness. The influence of porosity is shown in Fig. 12.

4.3.3 Test Equipment

Technical characteristics of the employed instrumentation at the first test site (Fig. 8b) were:

- ICP triaxial accelerometers with sensitivity (+ 10%) of 1 V/g, frequency range from 0.05 to 4000 Hz, resonant frequency > 10,000 Hz;
- uniaxial velocimeters with linear response in the 14–1.000 Hz band and sensitivity of 28.8 V/g;
- semi-circular flat jack sized 350×260 mm, 6 mm thickness and maximum operating pressure of 40 MPa;
- Europress hydraulic pump PL131 incorporating a pressure gauge with a resolution of 0.1 MPa;
- 1 DEMEC mechanical strain gauge for displacement measurements, integrating a digital indicator with a resolution of 0.001 mm.

For the second test, only triaxial accelerometers were employed for the acoustic emission measurement (Fig. 8c). In addition, measurement of displacements and pressure provided by the pump was digitalised by respectively adopting three GEFTRAN potentiometric displacement transducers (model PY-2-F-025-S03M) and one GEFTRAN pressure

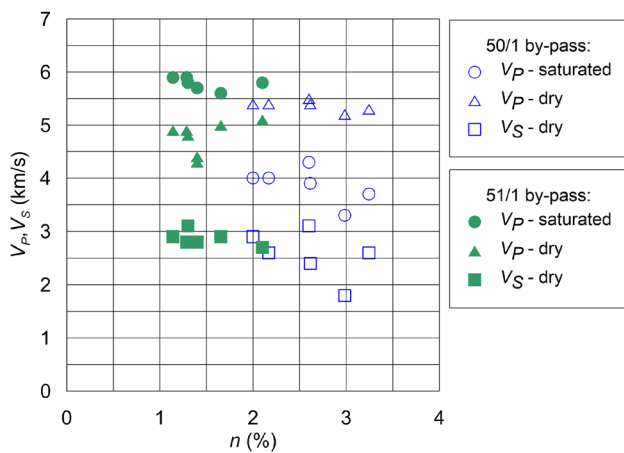


Fig. 10 P- and S-wave velocity against total porosity of the materials collected at the two sites

sensor (model TPSA) with a maximum operating value of 100 MPa.

A high sampling rate (to the order of 2000 Hz) was adopted to acquire accelerometric and velocimetric data. Automatic measurements of pressure and displacements were recorded every 0.01 s in the second test.

4.4 Results of the Newly Proposed In Situ Tests

A preliminary single flat jack test was performed to estimate the tangential stress at the tunnel side-wall, resulting in the value of 4.25 MPa in the first test (Fig. 13a). A significantly higher value, equal to 25.3 MPa, was obtained in the second test (Fig. 13b), possibly associated with the better quality of the rock material and consequently of the rock-mass, at this location.

The following stage of the test conducted with two flat jack tests was carried out with fixed pressure increments, maintained for a discrete amount of time for the detection of possible new fractures across the rock surface. In particular, in the first test the pressure was incrementally increased by 2 MPa, each level being maintained for 5 min. In the second test, due to the much higher recovery pressure detected during the compression stage with the single flat jack, three initial increments of 10 MPa were applied, the first two applied for only 1 min and the latter one for 5 min. Then, in the following steps the pressure was increased by 1 MPa, each level being maintained for 5 min, up to a pressure of 44 MPa. At this latter point the system started to lose pressure and oil leaks were evident near the flat jacks.

The recorded data were processed as follows:

- determination of the frequency content of the signals (accelerometric measurements were preferred at this

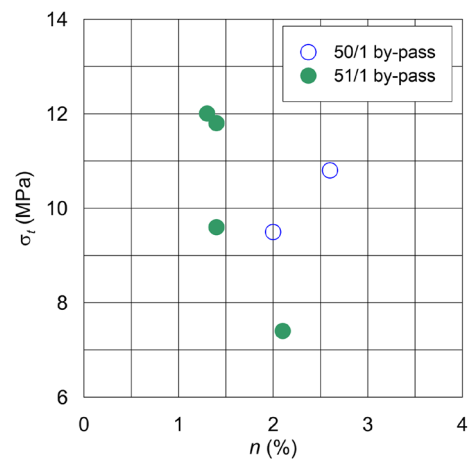


Fig. 11 Tensile strength versus total porosity

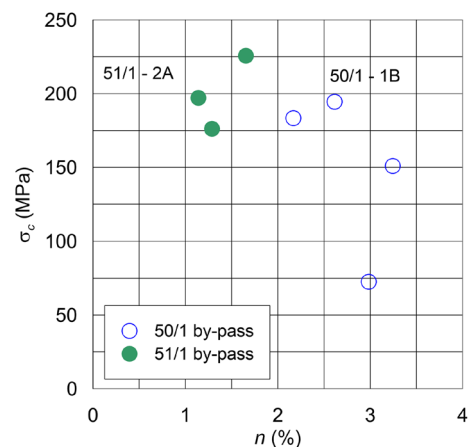


Fig. 12 Uniaxial compressive strength versus total porosity

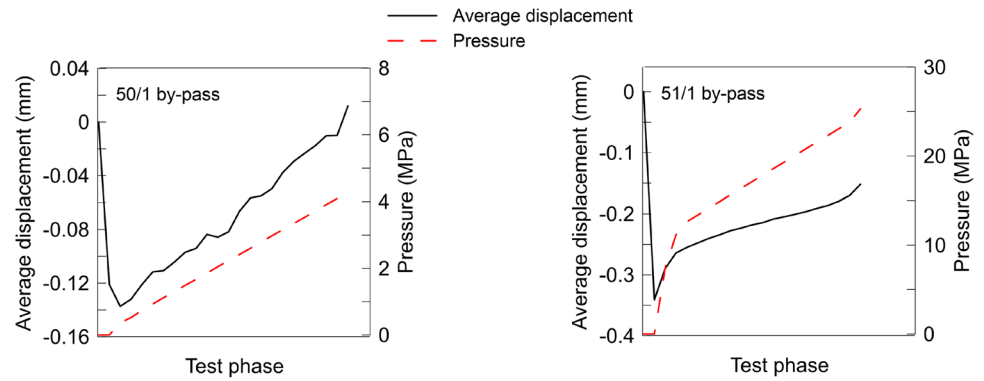
stage due to their better performance at high frequencies);

- notch filtering in the 50 Hz band to eliminate the undesired frequency intervals (and multiple tonal components);
- determination of the PSD_{max} over fixed time intervals;
- correlation of the energy content of the measured acoustic emissions with the pressure imposed by the two flat jacks and displacement measurements.

For the PSD_{max} assessment, a time window of 30 s was selected for the first test, increased to 60 s in the second test due to its likely longer duration. In both cases, an overlapping of 10% of adjacent time windows was implemented to improve the measurement interpretation in the frequency domain.

Figure 14 compares the pressure–displacement curves for the two tests. The much stiffer response of the rock-mass in the second test and the higher applied pressure are evident,

Fig. 13 Results of the single flat jack compression stage of the test: **a** 50/1 and **b** 51/1 by-pass



in contrast to the first experiment. In both cases a residual displacement was detected at the end of the test, even if the automatic instrumentation used for the pressure and displacement measurement in the 51/1 by-pass allowed a much more reliable description of the unloading stage.

The analysis of acoustic emission measurements also highlighted a different behaviour of the rock-mass before failure (Fig. 15). In the first test, the peaks in the PSD functions were always concentrated around 750 Hz, while in the second case two different areas with almost comparable acoustic emission intensity were observed, one at frequencies slightly over 500 Hz and the second one slightly over 900 Hz.

The correlation between acoustic emission development and applied pressure is shown in Fig. 16. More specifically, for the test in the 51/1 by-pass, values of PSD_{max} , obtained as the sum of the two peaks observed in the two frequency intervals discussed above, are plotted in this figure. The curves clearly show an increase in the emitted peak acoustic waves in the last part of the test soon before the maximum applied pressure. In particular, the higher values of PSD_{max} recorded in the first test at a pressure of about 14 MPa, reached the level of 0.5–0.6 (mg^2/Hz); in the second test the PSD_{max} quantity was in the range of 0.9–1.2 (mg^2/Hz) at a pressure of 38 MPa. In both cases the acoustic emission intensity starts to clearly decrease before the application of the maximum pressure, with further decrements in the unloading stage, especially in the second test.

A careful survey of the tunnel surface around the tested area in the 50/1 by-pass highlighted the presence of new fractures generated during the rock-mass compression with the double flat jacks (Fig. 17). Similar evidence was not found at the 51/1 site, the experiment being stopped before the macroscopic rupture of the rock-mass for technical problems related to the very high applied pressure. However, both the residual displacement shown in Fig. 16 and the trend displayed in the PSD_{max} time evolution suggest that failure mechanisms developed inside the rock-mass, making these experimental results consistent with those characterising the first experiment.

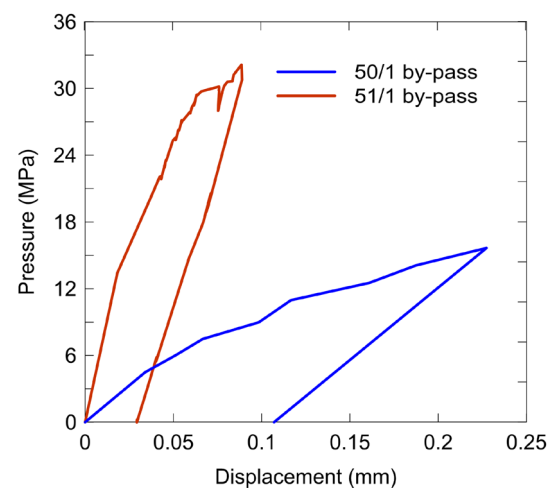


Fig. 14 Results of the double flat jack compression stage of the tests: applied pressure versus average displacement

Analysis of the acoustic emissions recorded in the post-peak stage indicated a different frequency content of the signals, with peaks concentrating around 200 Hz (Voza et al. 2019).

5 The Mules Method

The newly proposed in situ tests provided valuable input for the calibration of the rock-burst alarm threshold. A comprehensive methodology, denoted as the “Mules method” from the name of the construction lot (Voza et al. 2020a), was developed according to the flowchart reported in Fig. 18.

The core of the procedure consists in the interpretation of the in situ tests in terms of $PSDS$, in accordance with the time window selected for the analysis of monitoring data. As already discussed in paragraph 4.2, the time window was fixed at 24 h in 2017, 12 h in 2018 and 6 h in 2019, to better manage the more rapid evolution of monitoring measurements detected in that year.

Fig. 15 Frequency content of the signals recorded before failure

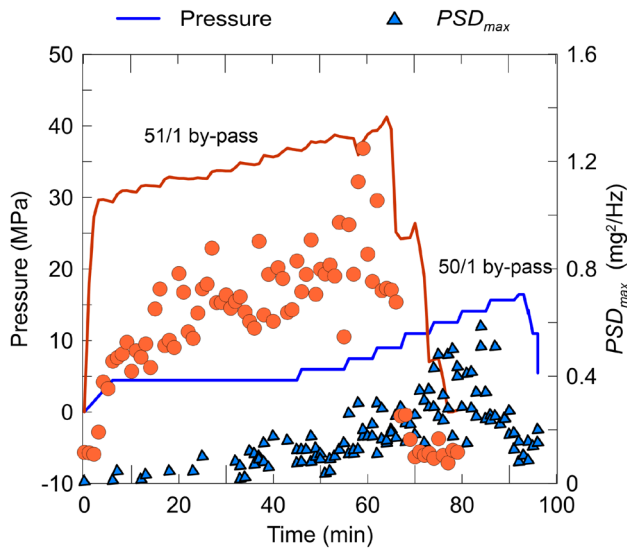
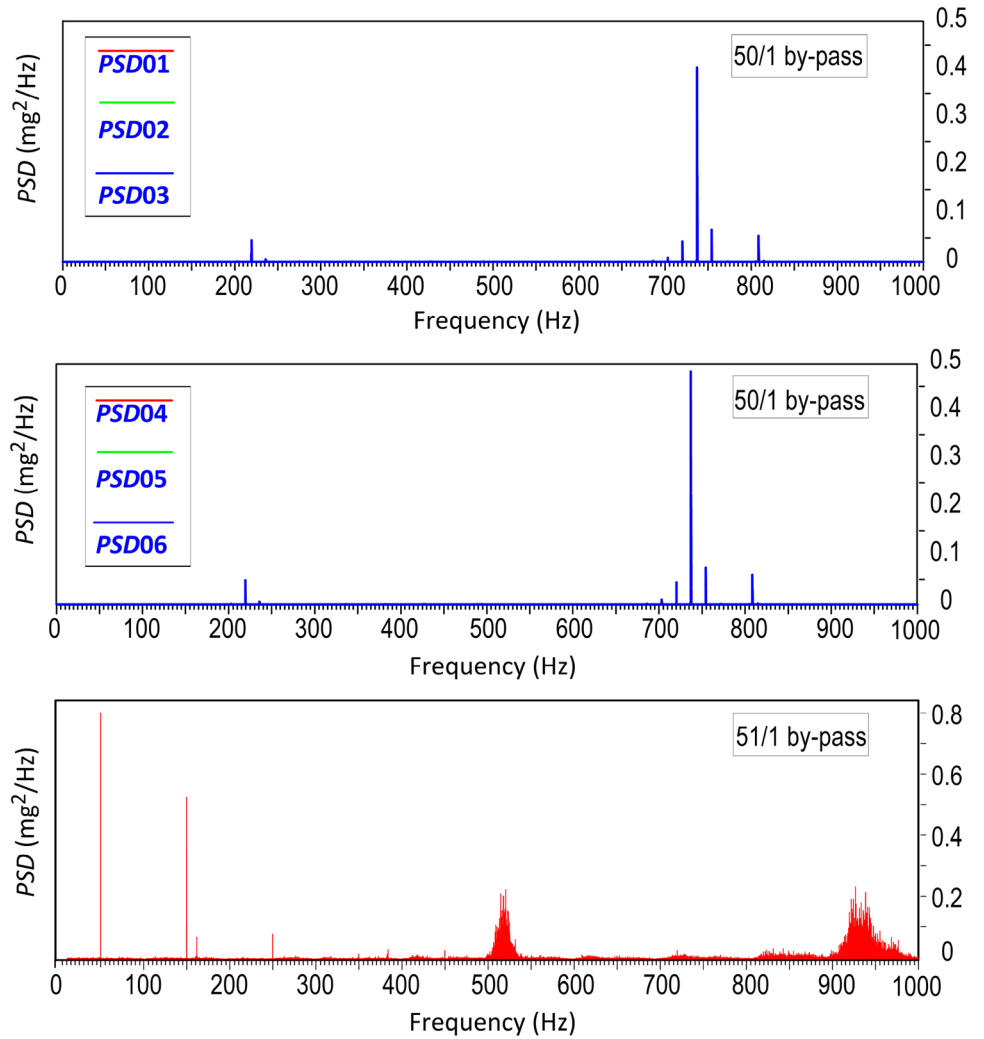


Fig. 16 Results of the double flat jack compression stage of the tests: evolution of applied pressure and PSD_{max} over time



Fig. 17 Evidence of fractures at the end of the first test conducted in the 50/1 by-pass

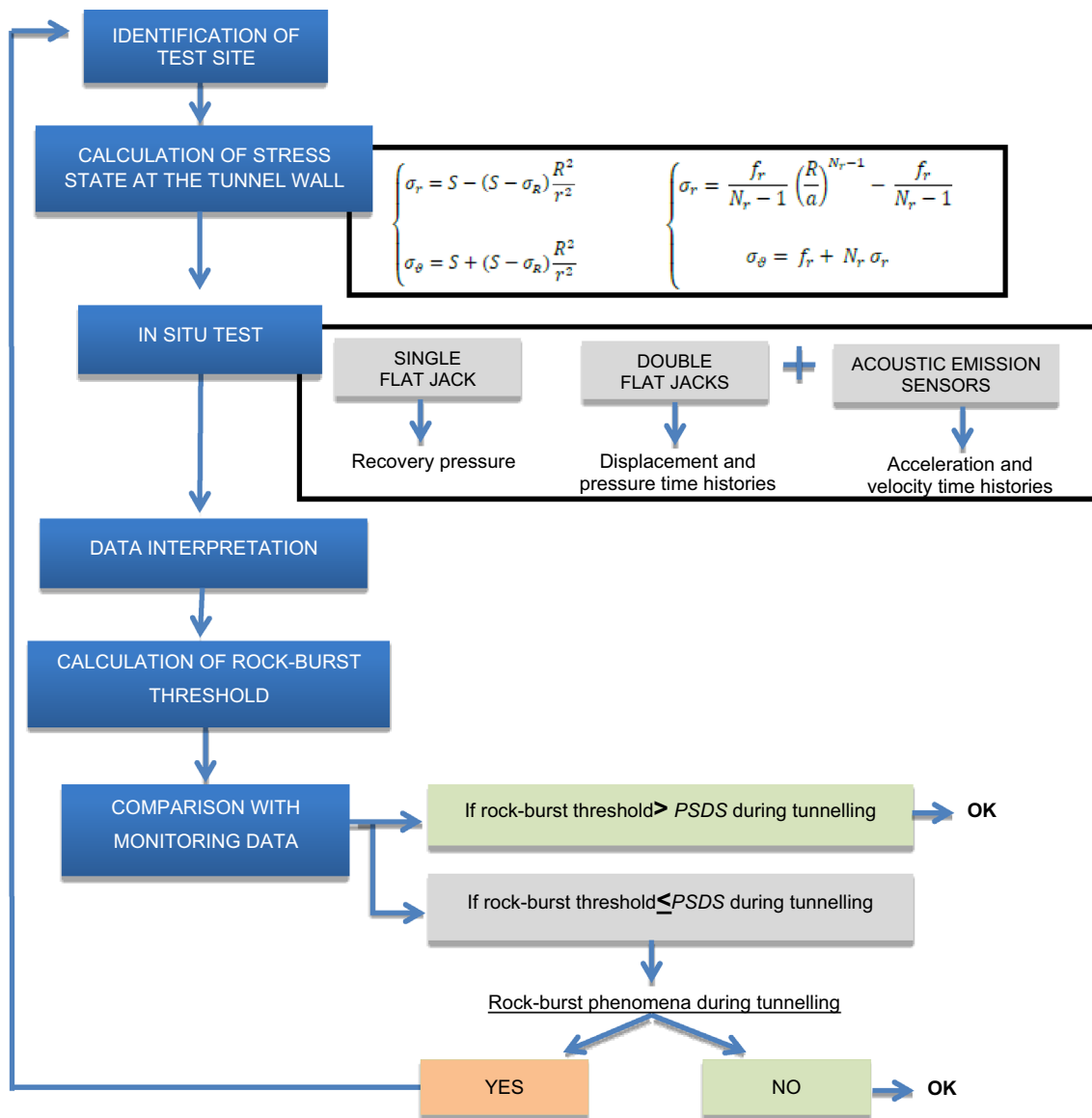


Fig. 18 Flowchart for the assessment of the rock-burst alarm threshold using the new in situ test results

Figures 5, 6 and 7 illustrate the comparison between the discussed threshold and the $PSDS$ values resulting from the acoustic emission data collected during the excavation.

The first test provided values of PSD_{max} between 0.5 and 0.6 (mg^2/Hz) over 30-s time intervals. Considering that the 2018 time window of 12 h contains 1440 intervals of 30 s each, the $PSDS$ quantity was calculated by multiplying the identified range of 0.5–0.6 by this number, obtaining a corresponding range of 720–846 (mg^2/Hz), respectively. This first determination was instrumental in defining for the year 2018 a lower alarm threshold for the rock-burst risk equal to 700 (mg^2/Hz), instead of the larger one considered in 2017 on a purely empirical basis.

The second test provided similar results, since the PSD_{max} values between 0.9 and 1.2 (mg^2/Hz) were collected over time windows of 60 s each, corresponding to 720 intervals within 12 h and to a $PSDS$ range of 648–864 (mg^2/Hz).

As such and also in agreement with the monitoring data and the safe construction of the tunnels, the same threshold was maintained also for the year 2019; however, due to the lower 6-h time window selected for this year, the value of $PSDS$ was halved and set equal to 350 (mg^2/Hz).

6 Conclusive Remarks and Perspectives

The paper described a novel in situ test developed for the assessment of the rock-burst alarm threshold during tunnelling. The experimental methodology was successfully applied to a stretch of the BBT system excavated in a granite rock-mass at elevated depths, affected during the tunnel excavation by few moderate spalling events.

The proposed test is relatively simple and inexpensive and easily implementable in the context of underground constructions. As regards the example discussed, it was carried out in a by-pass between the two main tunnels, so as to not interfere with the regular construction site activities.

The two experiments, conducted in the same granite formation but with different mechanical characteristics, highlighted the test repeatability in terms of maximum values of *PSD* before the failure and frequency content of the signals before and after failure. These results provided a valuable confirmation of the selected alarm threshold at the site, modified after the first test, also in agreement with the observations collected from the monitoring data and the construction works. The second experiment highlighted a shortcoming in the testing procedure in relation to the limited capacity of the two flat jacks in producing the complete failure of the hard and resistant rock-mass. Future research is thus aimed at finding alternative solutions for the mechanical part of the experiment, while maintaining the idea of monitoring the acoustic waves emitted by the rock-mass with geophones/accelerometers located at the tunnel wall.

The whole approach, which after the fact became known as the “Mules method”, allowed completion of the tunnel segments at risk of rock-burst with no serious accidents and with only very limited time delays. However, further experiments are required to validate this proof of concept in other geological and geomechanical contexts. In addition, especially for construction sites potentially affected by fragile failure phenomena of different intensity, it would be desirable to identify and assess an additional hazard index to differentiate large sudden events from clusters of small events with the same cumulative energy over the selected time interval (i.e. with the same value of *PSDS*).

Acknowledgements The authors wish to thank Mr. Stefano Fuoco, previous project manager of BBT Mules 2–3 lot and currently at Inferrail Firenze, and Mr. Domenico Buttafoco, project engineer at Brenner Tunnel Construction Scarl, for having constructively participated in the initial stages of the activity. Language support provided by the BBT-SE Settore Traduzioni in the person of Ms. Lisa Terzariol was very valuable for the preparation of the final version of the paper. The development of this methodology represents a very effective example of synergy among Client, Contractor and University for the improvement of safety of tunnel construction.

Funding Open access funding provided by Università degli Studi di Roma La Sapienza within the CRUI-CARE Agreement. No funding was received for conducting this study.

Data Availability Data are available on request.

Declarations

Conflict of Interest The authors have no competing interests to declare that are relevant to the content of this article.

Open Access This article is licensed under a Creative Commons Attribution 4.0 International License, which permits use, sharing, adaptation, distribution and reproduction in any medium or format, as long as you give appropriate credit to the original author(s) and the source, provide a link to the Creative Commons licence, and indicate if changes were made. The images or other third party material in this article are included in the article's Creative Commons licence, unless indicated otherwise in a credit line to the material. If material is not included in the article's Creative Commons licence and your intended use is not permitted by statutory regulation or exceeds the permitted use, you will need to obtain permission directly from the copyright holder. To view a copy of this licence, visit <http://creativecommons.org/licenses/by/4.0/>.

References

- Alcott JM, Kaiser PK, Simser BP (1998) Use of microseismic source parameters for rockburst hazard assessment. *Pure Appl Geophys* 153:41–65
- Boldini D, Bruno R, Egger H, Stafisso D, Voza A (2018) Statistical and geostatistical analysis of drilling parameters in the Brenner Base Tunnel. *Rock Mech Rock Eng* 51(6):1955–1963
- Brauner G (1994) Rockbursts in coal mines and their prevention. Balkema
- Cai M (2013) Principles of rock support in burst-prone ground. *Tunn Undergr Space Technol* 36:46–56
- Cai M, Kaiser PK (2018) Rockburst support reference book, vol 1 rockburst phenomenon and support characteristics MIRARCO-mining innovation. Laurentian University
- Cai W, Bai X, Si G, Cao W, Gong S, Dou L (2020) A monitoring investigation into rock burst mechanism based on the coupled theory of static and dynamic stress. *Rock Mech Rock Eng* 53:5451–5471
- Cheng W, Wang W, Huang S, Ma P (2013) Acoustic emission monitoring of rockbursts during TBM-excavated headrace tunneling at Jinping II hydropower station. *J Rock Mech Geotech Eng* 5:486–494
- Cook NGW (1963) The seismic location of rockbursts. In: *Proc. 5th Rock Mechanics Symposium*. Pergamon Press, Oxford, pp 493–518
- Diederichs MS (2007) The 2003 Canadian geotechnical colloquium: mechanistic interpretation and practical application of damage and spalling prediction criteria for deep tunnelling. *Can Geotech J* 44(9):1082–1116
- Dou L, Cai W, Cao A, Guo W (2018) Comprehensive early warning of rock burst utilizing microseismic multi-parameter indices. *Int J Min Sci Technol* 28:767–774
- Du K, Li X, Tao M, Wang S (2020) Experimental study on acoustic emission (AE) characteristics and crack classification during rock fracture in several basic lab tests. *Int J Rock Mech Min Sci* 133:104411
- Feng XT, Feng GL (2018) Dynamic and quantitative warning of rockbursts in tunnels using the in situ monitored microseismicity. In:

- Feng (ed) Rockburst. Mechanisms, monitoring, warning, and mitigation, subchapter 12.3. Butterworth-Heinemann
- Feng GL, Feng XT, Chen BR, Xiao YX, Yu Y (2015) A microseismic method for dynamic warning of rockburst development processes in tunnels. *Rock Mech Rock Eng* 48:2061–2076
- Feng XT, Yu Y, Feng GL, Xiao YX, Chen B, Jiang Q (2016) Fractal behaviour of the microseismic energy associated with immediate rockbursts in deep, hard rock tunnels. *Tunn Undergr Space Technol* 51:98–107
- Feng GL, Xia GQ, Chen BR, Xiao YX, Zhou RC (2019) A method for rockburst prediction in the deep tunnels of hydropower stations based on the monitored microseismicity and an optimized probabilistic neural network model. *Sustainability* 11:3212
- Feng GL, Lin M, Yu Y, Fu Y (2020) A microseismicity-based method of rockburst intensity warning in deep tunnels in the initial period of microseismic monitoring. *Energies* 13:2698
- Foderà GM, Voza A, Barovero G, Tinti F, Boldini D (2020) Factors influencing overbreak volumes in drill-and-blast tunnel excavation. A statistical analysis applied to the case study of the Brenner Base Tunnel—BBT. *Tunn Undergr Space Technol* 105:103475
- Frid V (2001) Calculation of electromagnetic radiation criterion for rockburst hazard forecast in coal mines. *Pure Appl Geophys* 158:931–944
- Frid V, Vozoff K (2005) Electromagnetic radiation induced by mining rock failure. *Int J Coal Geol* 64:57–65
- Ge M (2005) Efficient mine microseismic monitoring. *Int J Coal Geol* 64:44–56
- Hardy HR (1981) Applications of acoustic emission techniques to rock and rock structures: a state-of-the-art review. In: Drnevich, Gray (eds) *Acoustic emissions in geotechnical engineering practice*, Philadelphia. ASTM Special Technical Publication, pp 4–92
- He ZL, Lu CP, Zhang XF, Guo Y, Wang C, Zhang H, Wang BQ (2022) Research on mechanisms and precursors of slip and fracture of coal-rock parting-coal structure. *Rock Mech Rock Eng* 55:1343–1359
- Hoek E, Brown ET (1980) *Underground excavations in rock*. Institution of Mining and Metallurgy, London
- Hoek E, Diederichs MS (2006) Empirical estimation of rock mass modulus. *Int J Rock Mech Min Sci* 43:203–215
- ITA (2017) TBM excavation of long and deep tunnels under difficult rock conditions. ITA Report no. 19, p 64
- Kaiser E (1950) A study of acoustic phenomena in tensile test. PhD thesis, Technische Hochschule Munchen, Munich, Germany
- Kaiser PK, Tannant DD, McCreath DR (1996) *Canadian rockburst support handbook*. Geomechanics Research Centre Laurentian University Sudbury, p 314
- Kao CS, Carvalho FCS, Labuz JF (2011) Micromechanics of fracture from acoustic emission. *Int J Rock Mech Min Sci* 48:666–673
- Li S, Feng XT, Li Z, Chen B, Zhang C, Zhou H (2012) In situ monitoring of rockburst nucleation and evolution in the deeply buried tunnels of Jinping II hydropower station. *Eng Geol* 137–138:85–96
- Liang W, Sari A, Zhao G, McKinnon S, Wu H (2020) Short-term rockburst risk prediction using ensemble learning methods. *Nat Hazards* 104:1923–1946
- Liu JP, Feng XT, Li YH, Xu SD, Sheng Y (2013) Studies on temporal and spatial variation of MS activities in a deep metal mine. *Int J Rock Mech Min Sci* 60:171–179
- Liu X, Liu Z, Li X, Gong F, Du K (2020a) Experimental study on the effect of strain rate on rock acoustic emission characteristics. *Int J Rock Mech Min Sci* 133:104420
- Liu J, Wang R, Lei G, Si Y, Xu S, Li Y (2020b) Studies of stress and displacement distribution and the evolution law during rock failure process based on acoustic emission and microseismic monitoring. *Int J Rock Mech Min Sci* 132:104384
- Lockner D (1993) The role of acoustic emission in the study of rock fracture. *Int J Rock Mech Min Sci Geomechs Abstr* 30(7):883–899
- Mansurov VA (1994) Acoustic emission from failing rock behaviour. *Rock Mech Rock Eng* 27(3):173–182
- Marrazzo R (2020) *Analisi delle emissioni acustiche durante prove di compressione uniassiale su provini di granito di Bressanone*. Master thesis in Ingegneria per l'Ambiente e il Territorio, University of Bologna, Bologna, Italy (**in Italian**)
- Mendecki AJ (1997) *Seismic monitoring in mines*. Chapman & Hall, London
- Naji AM, Rehman H, Emad MZ, Ahmad S, Kim JJ, Yoo H (2019) Static and dynamic influence of the shear zone on rockburst occurrence in the headrace tunnel of the Neelum Jhelum hydropower project Pakistan. *Energies* 12:2124
- Obert L (1975) The microseismic method: discovery and early history. In: *Proc. 1st Conference of Acoustic Emission/Microseismic Activity in Geological Structures and Materials*. Trans. Tech. Publications, Clausthal-Zellerfeld, pp 11–12
- Ortlepp WD, Stacey TR (1994) Rockburst mechanisms in tunnels and shafts. *Tunn Undergr Space Technol* 9(1):59–65
- Padovese P, Berti A, Baldovin E, De Paola A, Morelli GL, Buraschi L, Ascari G (2017) *Innovazioni delle tecnologie di scavo meccanizzato in ammassi rocciosi caratterizzati da roccia dura con distacchi in calotta e alte coperture*. 16° Ciclo di Conferenze di Meccanica e Ingegneria delle Rocce, February 16–17, Turin, p 20
- Qiu L, Liu Z, Wang E, He X, Feng J, Li B (2020) Early-warning of rock burst in coal mine by low-frequency electromagnetic radiation. *Eng Geol* 279:105755
- Siboni M (2019) *Studio dei valori di soglia di rischio di rockburst ottenuti mediante una nuova prova sperimentale nella galleria di base del Brennero*. Master thesis in Ingegneria per l'Ambiente e il Territorio, University of Bologna, Bologna, Italy (**in Italian**)
- Tao ZY (1988) *Support design of tunnels subjected to rockbursting*. Rock mechanical power plants. Balkema, Rotterdam, pp 407–411
- Valguarnera L (2018) *Metodo sperimentale per la determinazione della soglia di rischio rockburst nella Galleria di Base del Brennero*. Master thesis in Ingegneria Civile, University of Bologna, Bologna, Italy (**in Italian**)
- Voza A, Valguarnera L, Fuoco S, Ascari G, Boldini D, Buttafoco D (2019) Acoustic emissions from flat-jack test for rock-burst prediction. In: Peila et al. (eds) *Tunnels and underground cities: engineering and innovation meet archaeology, architecture and art*, pp 1199–1207
- Voza A, Valguarnera L, Ascari G, Boldini D (2020a) Rock-burst risk assessment by acoustic emission measurement and interpretation at the Brenner Base Tunnel: the “Mules method.” *Gallerie e Grandi Opere Sotterranee* 133:19–29
- Voza A, Valguarnera L, Fuoco S, Ascari G, Boldini D, Buttafoco D (2020b) A new methodology for the rock-burst assessment during tunnel construction. In: Calvetti et al. (eds) *Geotechnical Research for Land Protection and Development*, Lecture Notes in Civil Engineering, vol. 40, pp 668–677
- Yu Y, Zhu B, Guo H, Chen B, Geng D (2021) Warning index associated with rock burst in deeply buried tunnels. *Int J Geomech* 11:04021211
- Zhang CQ, Feng XT, Zhou H, Qiu SL, Wu WP (2013) Rockmass damage development following two extremely intense rockbursts in deep tunnels at Jinping II hydropower station, southwestern China. *Bull Eng Geol Env* 72:237–247